Electronic Supplementary Information

Controlling Phase Transition from Single-Layer MTe_2 (M=Mo, W): Modulation of Potential Barrier under Strain

H. H. Huang[a], Xiaofeng Fan[a, *], David J. Singh[a, c], Hong Chen [b],
Q. Jiang[a] and W.T. Zheng[a, †]

a. College of Materials Science and Engineering, Jilin University, Changchun 130012, China
b. Department of Control Science & Engineering, Jilin University, Changchun 130012, China
c. Department of Physics and Astronomy, University of Missouri, Columbia, Missouri 65211-7010, USA

*E-mail: xffan@jlu.edu.cn ; † E-mail: wtzheng@jlu.edu.cn

Table S1

	ΔE_1(eV)	ΔE_2(eV)	Barrier-1(eV/f.u)	Barrier-2(eV/f.u)
$MoTe_2$	0.091	0.047	0.893	0.842
WTe_2	0.049	0.035	0.767	0.740

Table 1 ΔE_1 is the energy difference of 2H phase calculated with 2H lattice parameters and with 1T' lattice parameters. ΔE_2 is the energy difference of 1T' phase calculated with 1T' lattice parameters and with 2H lattice parameters. Barrier-1 is the energy barrier from 2H to 1T' which is calculted with 2H lattice parameters. Barrier-2 is the energy barrier from 2H to 1T' which are calculted with 1T' lattice parameters.

Fig. S1

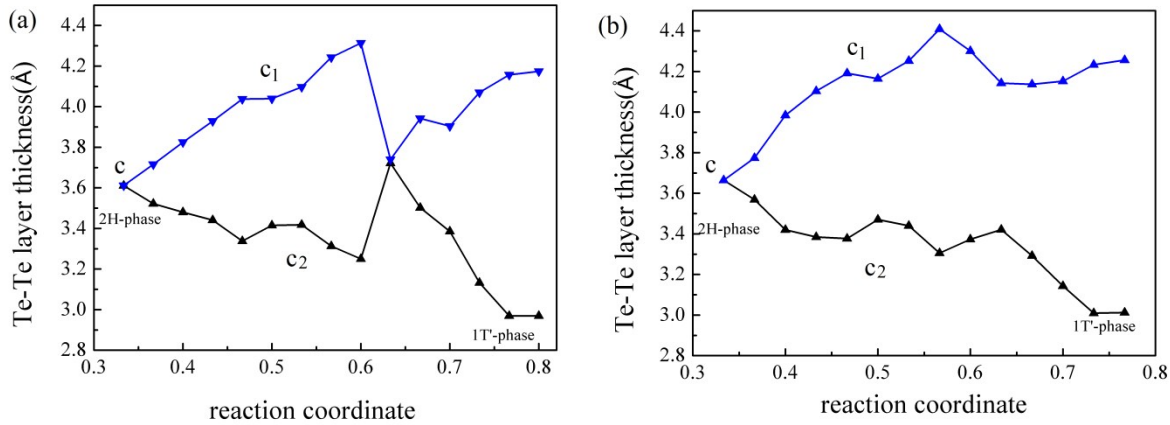

Fig. S1 Changes of lattice paramerter in *c*-axis indicated in Figure 1 following the minimum-emergy path way with reaction coordinate defined by the coorinate of the related Te atoms along *b* axis obtained in Figure 2 for the phase transtion from 2H to 1T' about $MoTe_2$ (a) and WTe_2 (b).

Fig. S2

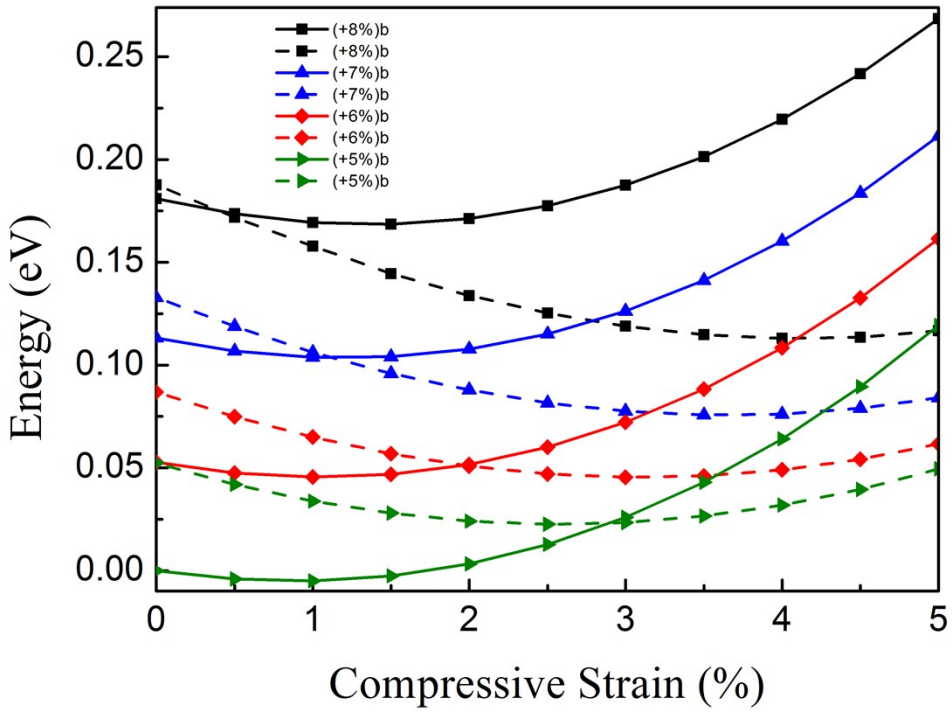

Fig. S2 Energy changes of 2H- and 1T'-phase $MoTe_2$ following the *a*-axis compression under different *b*-axis tensile strain from 5% to 8%. Note that solid line represents 2H structure and the dash line is for 1T'structure.

Table S2

	Tensile strain (b axis)	Compression of a-axis Energy minimum (2H-phase)	Compression of a-axis Energy minimum (1T'-phase)
	5%	1%	2.5%
$MoTe_2$	6%	1%	3%
	7%	1%	3.5%
	8%	1%	4%

Table S2 Under different tensile strain of *b*-axis, the *a*-axis compression at the equilibrium state for 2H-phase and 1T' phase of $MoTe_2$

Fig. S3

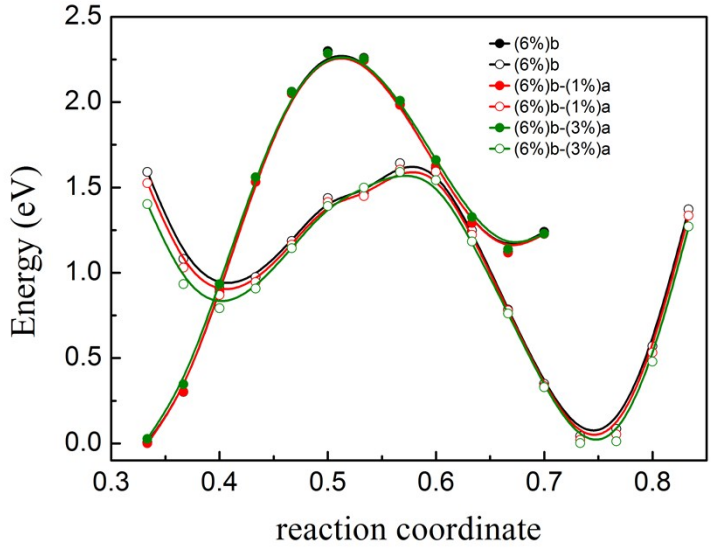

Fig. S3 Potential energy curves of initial state (metal atom fixed at 0.5 in *b* axis shown by solid circle lines) and final state (metal atom fixed at 0.36 in *b* axis shown by open circle lines) under *b*-axis tensile strain of 6% with different *a*-axis compression including 0%, 1% and 3% for $MoTe_2$.

Fig. S4

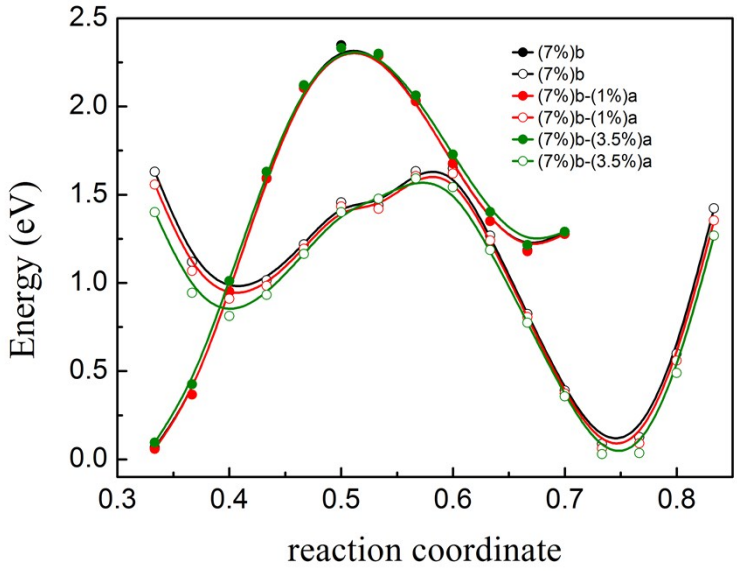

Fig. S4 Potential energy curves of initial state (metal atom fixed at 0.5 in *b* axis shown by solid circle lines) and final state (metal atom fixed at 0.36 in *b* axis shown by open circle lines) under *b*-axis tensile strain of 7% with different *a*-axis compression including 0%, 1% and 3% for $MoTe_2$.

Table S3

	Tensile strain (*b* axis)	Compression (*a* axis)	Energy barrier (eV/f.u.)
	6%	0	0.818
	6%	1%	0.802
$MoTe_2$	6%	3%	0.782
	7%	0	0.790
	7%	1%	0.780
	7%	3.5%	0.748

Table S3 Energy barriers from 2H to 1T' of $MoTe_2$ with diffirent *a*-axis compression. under different *b*-axis tensile strain

Fig. S5

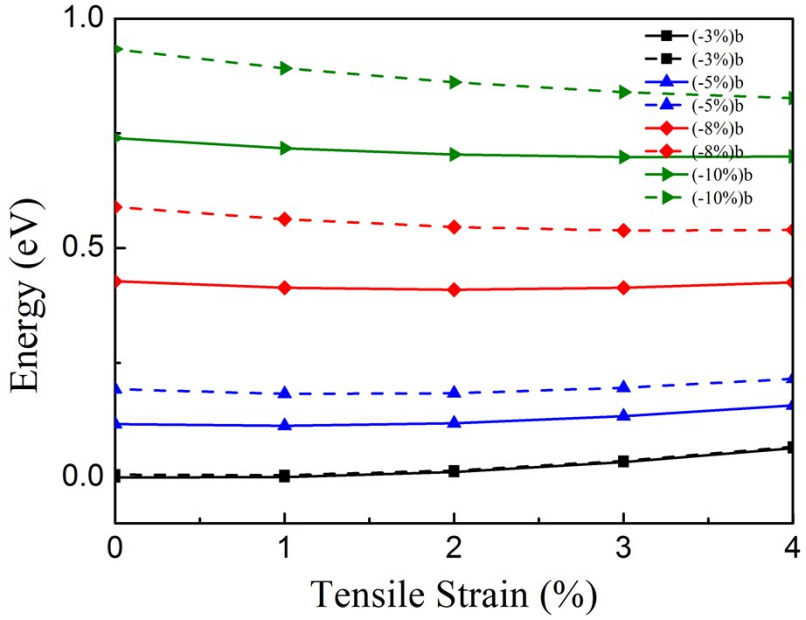

Fig. S5 Energy changes of 2H- and 1T'-phase WTe_2 following the *a*-axis expansion (tensile strain) under different *b*-axis compressive strain from -3% to -10%. Note that solid line represents 2H structure and the dash line is for 1T'structure.

Table S4

	Compressive strain (*b* axis)	Expansion (*a* axis) Energy minimum (2H-phase)	Expansion (*a* axis) Energy minimum (1T'-phase)
	3%	1%	1%
WTe_2	5%	1%	1%
	8%	2%	3%
	10%	3%	4%

Table S4 Under different compressive strain of *b*-axis, the *a*-axis expansion at the equilibrium state for 2H-phase and 1T' phase of WTe_2

Fig. S6

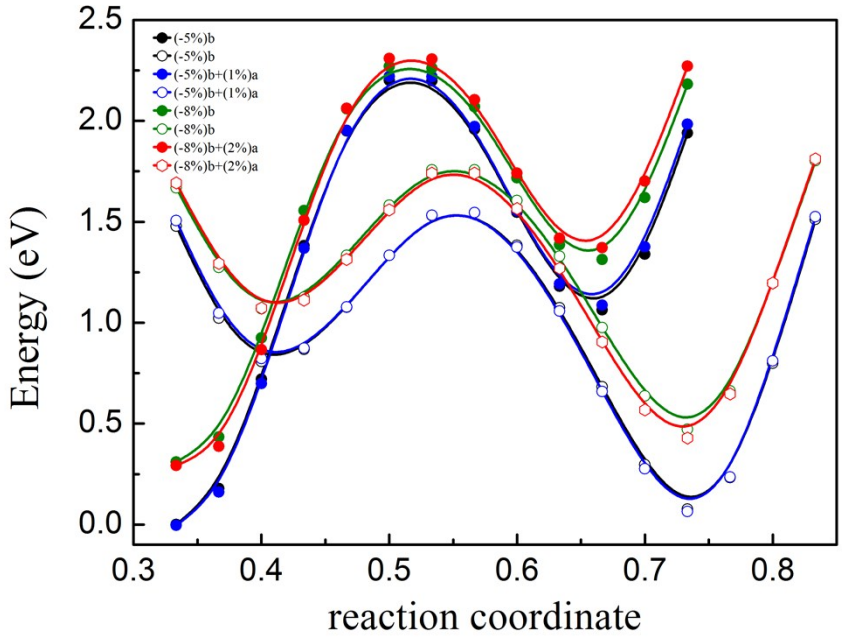

Fig. S6 Potential energy curves of initial state (metal atom fixed at 0.5 in *b* axis shown by solid circle lines) and final state (metal atom fixed at 0.36 in *b*-axis shown by open circle lines) under *b*-axis compressive strain of 5% with different a-axis expansion including 0% and 1% and under *b*-axis tensile strain of 8% with different *a*-axis expansion including 0% and 2% for WTe_2.

Table S5

	Compressive strain (*b* axis)	Expansion (*a* axis)	Energy barrier (eV/f.u.)
	5%	0	0.772
WTe_2	5%	1%	0.775
	8%	0	0.724
	8%	2%	0.724

Table S5 Energy barriers from 2H to 1T' of WTe_2 with diffirent *a*-axis expansion under different *b*-axis compressive strain

Fig. S7

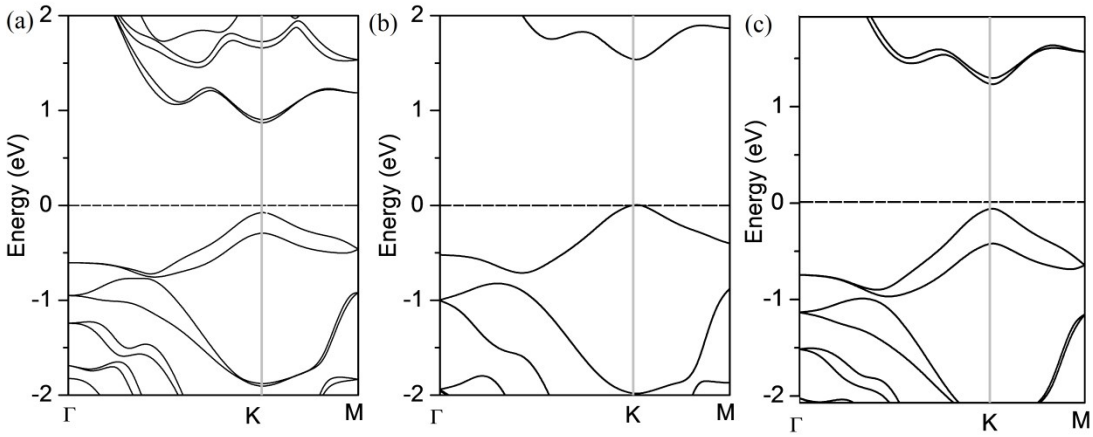

Fig. S7 Band structures of monolayer 2H-$MoTe_2$ calculated by PBE/GGA with spin-orbit coupling (a), HSE06 (b) and HSE06 with spin-orbit coupling

Fig. S8

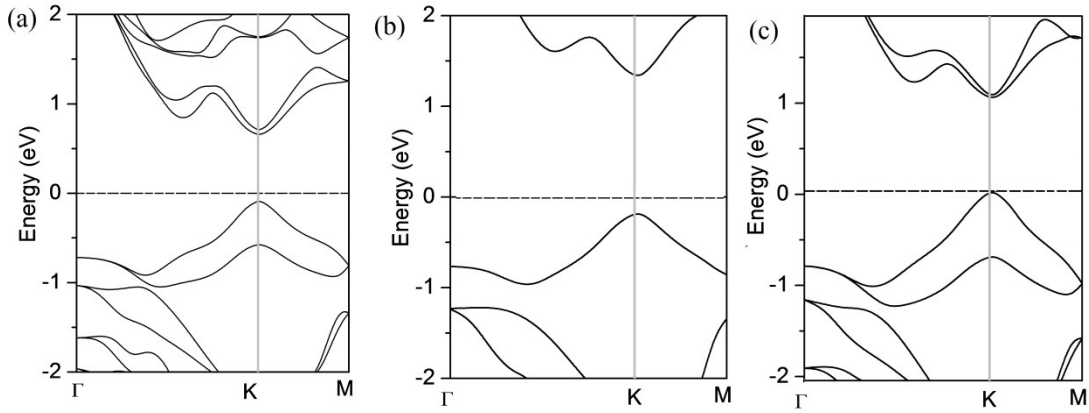

Fig. S8 Band structures of monolayer 2H-WTe_2 calculated by PBE/GGA with spin-orbit coupling (a), HSE06 (b) and HSE06 with spin-orbit coupling

Fig. S9

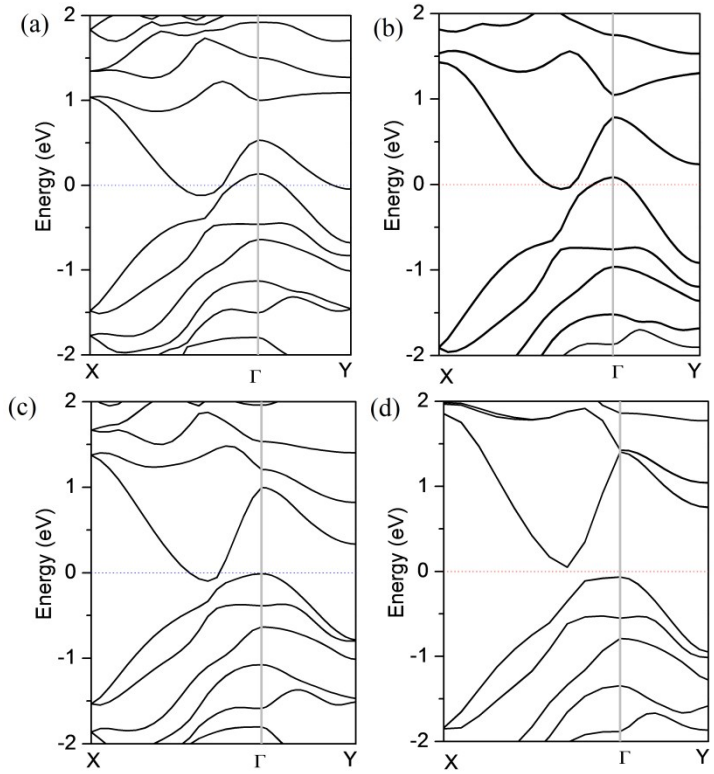

Fig. S9 Band structures of monolayer 1T-$MoTe_2$ (a, b) and 1T-$MoTe_2$ (c, d) calculated by PBE/GGA and HSE06with spin-orbit coupling, respectively